Spectrochimica Acta Part A: Molecular and Biomolecular Spectroscopy 159 (2016) 209–218

Contents lists available at ScienceDirect

Spectrochimica Acta Part A: Molecular and Biomolecular Spectroscopy

journal homepage: www.elsevier.com/locate/saa

# Spirolactone and spirothiolactone rhodamine-pyrene probes for detection of $Hg^{2+}$ with different sensing properties and its application in living cells

Qing-Qing Rui [a], Yi Zhou [a], Yuan Fang [a], Cheng Yao [a,b,*]

[a] College of Science, Nanjing Tech University, Nanjing 211816, China
[b] State Key Laboratory of Coordination Chemistry, Nanjing University, Jiangsu 210093, China

ARTICLE INFO

*Article history:*
Received 27 April 2015
Received in revised form 12 January 2016
Accepted 16 January 2016
Available online 20 January 2016

*Keywords:*
Fluorescent probe
$Hg^{2+}$ ion
Rhodamine B
Live-cell imaging

ABSTRACT

Two new rhodamine B-based fluorescent probes **PyRbS** and **PyRbO** containing pyrene moiety were designed and synthesized. Both of the probes showed colorimetric and fluorometric sensing abilities for $Hg^{2+}$ with high selectivity over other metal ions. The binding analysis using Job's plot suggested 1:1 stoichiometry for the complexes formed for $Hg^{2+}$. Compared with **PyRbO**, the **PyRbS** showed higher selectivity and sensitivity due to the thiophilic property of $Hg^{2+}$ ion. The **PyRbS** exhibited the linear fluorescence quenching to $Hg^{2+}$ in the range of 0.3 to 4.8 μM ($\lambda_{ex}$ = 365 nm) and 0.3 to 5.4 μM ($\lambda_{ex}$ = 515 nm), and the detection limit was 0.72 μM. Moreover, ratiometric changes of **PyRbS** with $Hg^{2+}$ in absorption spectrum were observed, which could not be obtained in the combination of **PyRbO** with $Hg^{2+}$. In addition, the methyl thiazolyl tetrazolium (MTT) assay demonstrated that **RbPyS** had low cytotoxicity and was successfully used to monitor intracellular $Hg^{2+}$ levels in living cells.



## 1. Introduction

Mercury pollution is a ubiquitous problem due to the inorganic mercury releasing into the environment through varieties of anthropogenic behavior (like coal and gold mining, combustion of fossil fuels and chemical industry) and natural sources (like volcanic eruption and forest fires) [1–3]. Mercury is harmful to photosynthesis and transpiration of plants, and it would pollute the environment [4,5].The inorganic mercury also can be transformed to $CH_3HgX$ species (X = halogen) by some prokaryotes that live in the underwater habitats [6]. Ultimately, methylmercury would be ingested by humans through mercury bioaccumulation [7]. To make things worse, mercury intoxication can lead to manifold neurological problems, such as prenatal brain damage, cognitive and motion disorders, vision and hearing loss, and death [8–10]. Therefore, the detection of mercury ion is of great significance.

In recent years, many conventionally quantitative approaches to the detection of $Hg^{2+}$ have been reported, such as chromatography [11–13], capillary electrophoresis [14–16], atomic absorption spectroscopy [17,18], etc. Because the above analysis methods require multistep sample pretreatment and/or sophisticated instrumentation, and they are not well-suited for the rapid detection or studies of $Hg^{2+}$ in vivo. The application of $Hg^{2+}$-sensitive small-molecule ligands provides remarkable optional response immediately, which can overcome the limitations that were mentioned above. Recently, colorimetric and fluorometric probes for the detection of $Hg^{2+}$ have attracted considerable attention, because of their operational simplicity, high selectivity, sensitivity, rapidity, low cost of equipment and direct visual perception [19–21].

In this paper, we developed two rhodamine-based probes, **PyRbS** and **PyRbO** consisting of pyrene fluorophore (Scheme 1). Both of them could be used for the detection of $Hg^{2+}$ with high sensitivity and selectivity, and showed colorimetric and fluorometric response in a short time. Because **PyRbS** contained sulfur atom, the thiophilic nature of $Hg^{2+}$ resulted in the advantageous properties of **PyRbS**. Moreover, pyrene moiety served successfully as a source of ratiometric absorption changes of **PyRbS** with $Hg^{2+}$. The low cytotoxicity and cell-membrane penetrability of **PyRbS** were confirmed by MTT assay and cell imaging, respectively.

## 2. Experimental section

### 2.1. Equipment and reagent

$^1H$ NMR and $^{13}C$ NMR were measured on a Bruker AV-400 or Bruker AV-300 spectrometer with chemical shifts reported in ppm (in $CDCl_3$; TMS as internal standard). Electrospray ionization mass spectra (ESI-MS) were analyzed on a LCTTM system. UV–visible spectra were recorded on a Perkin–Elmer 35 spectrometer and fluorescence spectra were measured on Perkin–Elmer LS 50B fluorescence spectrophotometer.

All the reagents and solvents (analytic grade) were purchased from commercial suppliers. Doubly distilled water was used in all of the

* Corresponding author at: College of Science, Nanjing Tech University, Nanjing 211816, China.
*E-mail addresses:* yaocheng@njtech.edu.cn, yaochengnjut@126.com (C. Yao).

http://dx.doi.org/10.1016/j.saa.2016.01.024
1386-1425/

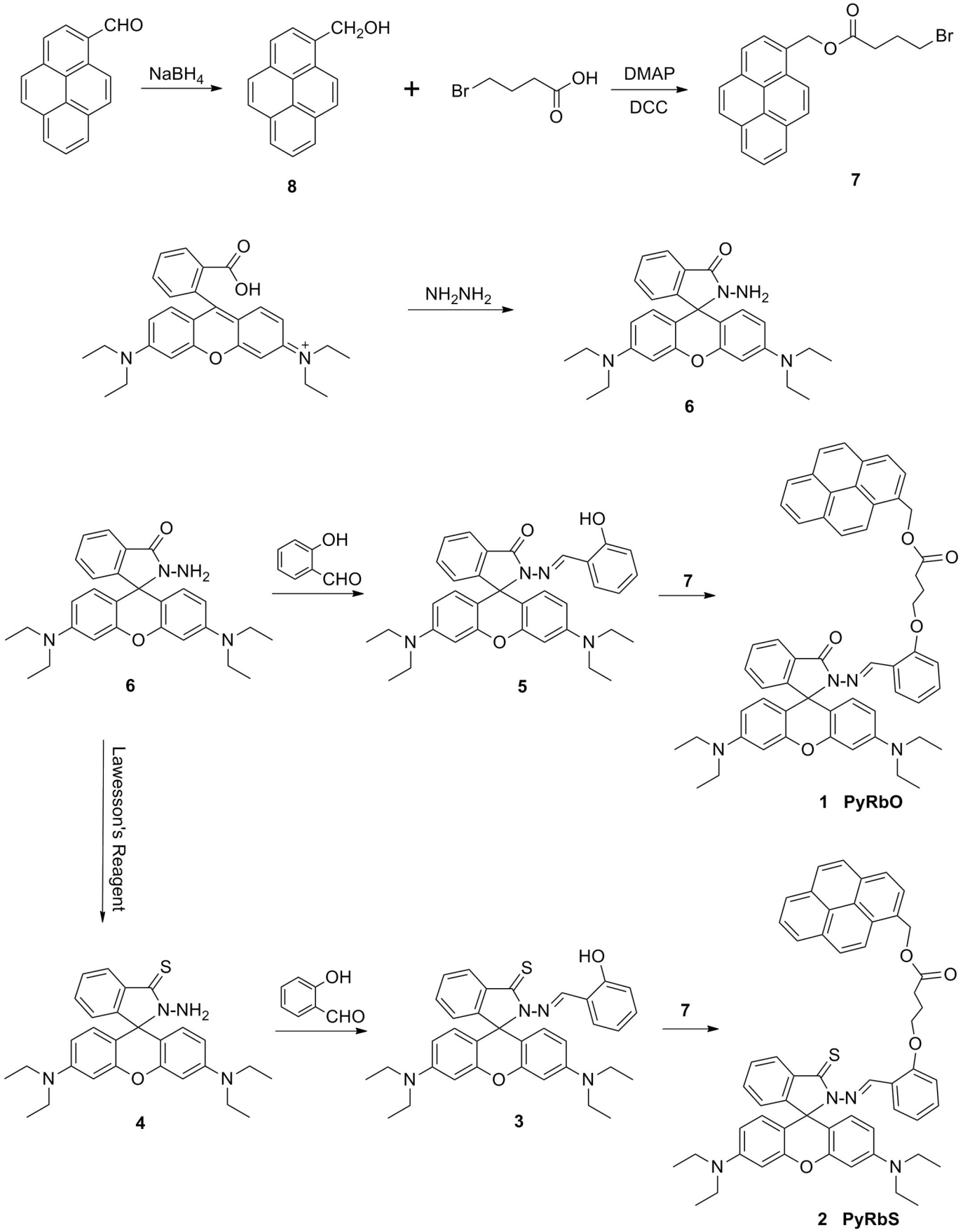


**Scheme 1.** Synthetic route of **PyRbO** and **PyRbO**.

experiments. Metal ions were prepared by $Hg(ClO_4)_2 \cdot 3H_2O$, $NaNO_3$, $KNO_3$, $Mg(NO_3)_2$, $Ca(NO_3)_2$, $Ni(NO_3)_2 \cdot 6H_2O$, $Ba(NO_3)_2$, $AgNO_3$, $Zn(NO_3)_2 \cdot 2H_2O$, $MnCl_2$, $CuSO_4$, $CdCl_2 \cdot H_2O$, $Pb(NO_3)_2$, $CrCl_3 \cdot 6H_2O$, $Co(NO_3)_2 \cdot 6H_2O$, $Al(NO_3)_3 \cdot 9H_2O$ and $FeCl_2 \cdot 4H_2O$.

### 2.2. Synthesis for probes

#### 2.2.1. Synthesis of 1-pyrenemethanol **8**

1-pyrenecarboxaldehyde (0.35 g, 1.50 mmol) was dissolved in 15 mL methanol, and $NaBH_4$ (0.08 g, 2.10 mmol) was added slowly into the reaction mixture at 0 °C for 30 min. After stirring at room temperature overnight, 20 mL 5% HCl was added in the reaction to quench the excess $NaBH_4$, and the solution changed to milk-white suspension. The organic solvent was removed and then the solid was extracted with ethyl acetate (3 × 15 mL). The organic fractions were washed with saturated $NaHCO_3$ aqueous solution. The collected organic solution was dried with sodium sulfate and was concentrated to give compound **8** in an 81% yield. $^1$H NMR (400 MHz, $CDCl_3$) δ 8.30–7.96 (m, 9 H, Ar–H), 5.33 (s, 2 H, $CH_2$). TOF-MS: m/z 231.1[M–H]$^-$.

#### 2.2.2. Synthesis of compound **7**

Compound **7** was synthesized according to the reported method [22]. $^1$H NMR (400 MHz, $CDCl_3$) δ 8.30–7.99 (m, 9 H, Ar–H), 5.86 (s, 2H, $CH_2$), 3.44 (t, $J$ = 6.5 Hz, 2 H, $CH_2$), 2.58 (t, $J$ = 7.2 Hz, 2 H, $CH_2$), 2.20 (t, $J$ = 6.8 Hz, 2 H, $CH_2$). TOF-MS: m/z 403.1, 405.1 [M + Na] $^+$.

#### 2.2.3. Synthesis of rhodamine B hydrazide **6**

Rhodamine B (2.00 g, 4.5 mmol) was dissolved in 150 mL dry ethanol, and 4.0 mL (excess) hydrazine hydrate (80%) was added dropwise in the reaction suspension with stirring at room temperature. Then, the mixture was refluxed at 85 °C for 2 h and evaporated to get orange solid. The solid was dissolved in diluted hydrochloric acid. The pH of the solution was adjusted with sodium hydroxide aqueous solution to 9–10. The appeared precipitate was filtered and washed with cold ethanol 3 times. After drying, the reaction afforded 1.44 g pink solid in a yield of 70%. $^1$H NMR (400 MHz, $CDCl_3$) δ 7.93 (t, $J$ = 4.4 Hz, 1H, Ar-H), 7.45 (t, $J$ = 4.2 Hz, 2H, Ar–H), 7.11 (t, $J$ = 4.2 Hz, 1H, Ar–H), 6.46 (d, $J$ = 8.8 Hz, 2H, Ar–H), 6.42 (d, $J$ = 2.5 Hz, 2H, Ar–H), 6.29 (dd, $J$ = 8.8, 2.6 Hz, 2H, Ar–H), 3.61 (s, 2H, $NH_2$), 3.34 (q, $J$ = 7.1 Hz, 8H, $CH_2$), 1.17 (t, $J$ = 7.0 Hz, 12H, $CH_3$). TOF-MS: m/z 457.3[M + H]$^+$, 479.3[M + Na]$^+$.

#### 2.2.4. Synthesis of compound **5**

Rhodamine hydrazide (**6**, 0.12 g, 0.16 mmol) was added in 40 mL dry methyl alcohol. Salicylic aldehyde (0.063 g, 0.52 mmol) was added and then the reaction was refluxed at 50 °C. After 12 h, the appeared pink precipitate was filtered and washed 3 times with cold methyl alcohol. After drying, the reaction afforded 0.09 g solid in a 62% yield. $^1$H NMR (400 MHz, $CDCl_3$) δ 10.83 (s, 1H, OH), 9.23 (s, 1H, N═CH), 7.98 (dd, $J$ = 6.4, 1.6 Hz, 1H, Ar–H), 7.58–7.48 (m, 2H, Ar–H), 7.20–7.14 (m, 2H, Ar–H), 7.10 (dd, $J$ = 7.7, 1.3 Hz, 1H, Ar–H), 6.86 (d, $J$ = 8.2 Hz, 1H, Ar–H), 6.78 (t, $J$ = 7.1 Hz, 1H, Ar–H), 6.49 (d, $J$ = 9.1 Hz, 4H, Ar–H), 6.26 (dd, $J$ = 8.9, 2.5 Hz, 2H, Ar–H), 3.32 (q, $J$ = 7.0 Hz, 8H, $CH_2$), 1.15 (t, $J$ = 7.0 Hz, 12H, $CH_3$). TOF-MS: m/z 583.3[M + Na]$^+$.

#### 2.2.5. Synthesis of probe **1** (***PyRbO***)

Compound **5** (0.28 g, 0.5 mmol), compound **7** (0.57 g, 1.5 mmol), potassium carbonate (0.69 g, 5 mmol) and small amount of potassium iodide were mixed in 30 mL dry acetone and stirred under reflux conditions for 12 h. The suspension was filtered, and then the solution was evaporated. The residue was purified by flash chromatography (EA/PE, 1:2, v/v) as eluant to afford 0.13 g light yellow product in a yield of 30%. $^1$H NMR (400 MHz, $CDCl_3$) δ 8.45 (s, 1H, N═CH), 8.32 (d, $J$ = 9.2 Hz, 1H, Ar–H), 8.20 (dd, $J$ = 13.7, 6.4 Hz, 2H, Ar–H), 8.16–8.10 (m, 3H, Ar–H), 8.08 (d, $J$ = 6.7 Hz, 2H, Ar–H), 8.04 (d, $J$ = 7.7 Hz, 1H,

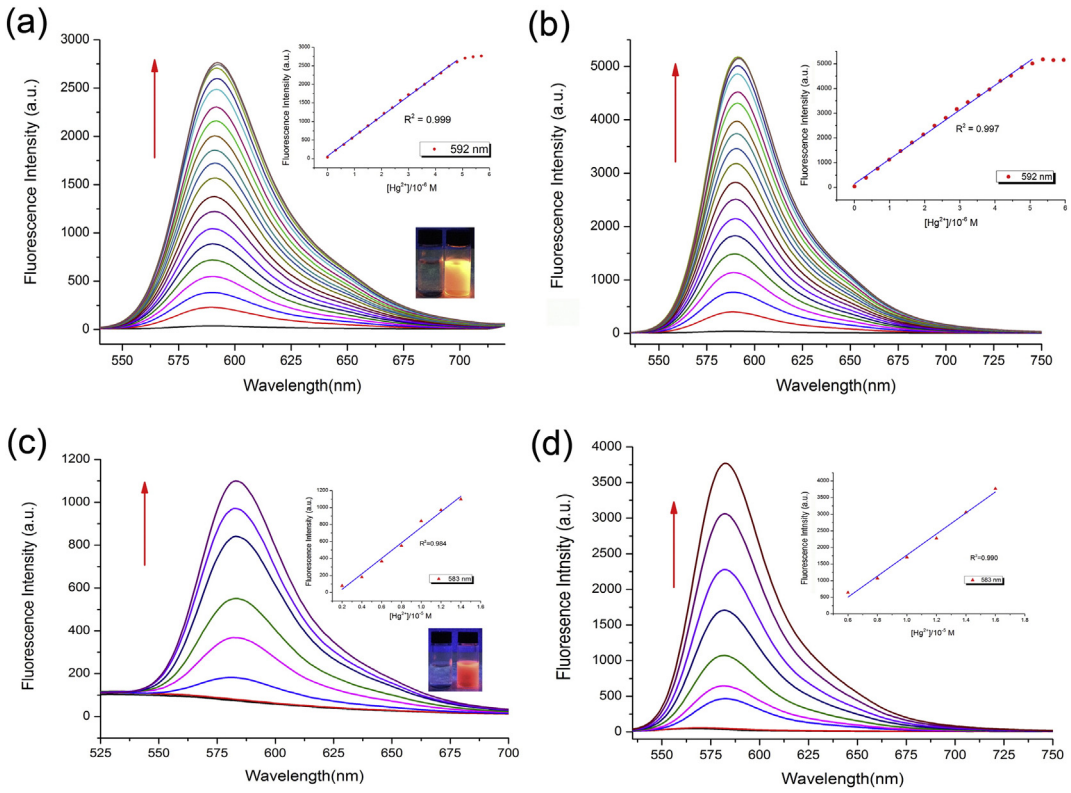


**Fig. 1.** (a) and (b) Fluorescence spectra of **PyRbS** (5 μM) in EtOH/$H_2O$ (2:1, v/v) with various amount of $Hg^{2+}$ (0–6 μM). Inset: the fluorescence intensity at 592 nm. (a) $\lambda_{ex}$ = 365 nm. (b) $\lambda_{ex}$ = 515 nm. (c) and (d) Fluorescence spectra of **PyRbO** (10 μM) in EtOH with various amount of $Hg^{2+}$ (0–16 μM). Inset: the fluorescence intensity at 583 nm. (c) $\lambda_{ex}$ = 365 nm. (d) $\lambda_{ex}$ = 515 nm.

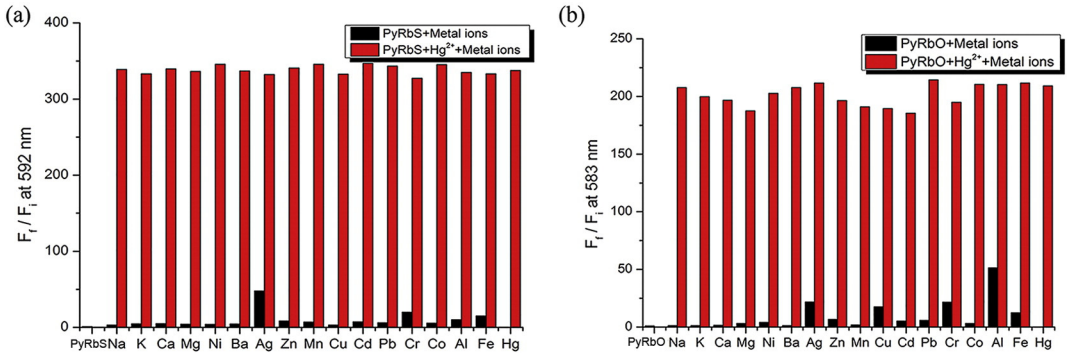


**Fig. 2.** (a) Fluorescence changes of 5 μM **PyRbS** in the presence of various metal ions in EtOH/$H_2O$ (2:1, v/v) at 592 nm. Bars represent the final fluorescence intensity ($F_f$) over the initial fluorescence intensity ($F_i$) at $\lambda_{ex} = 515$ nm. Black bars represent the fluorescence intensity of 5 μM **PyRbS** with various competing metal ions (4.0 equiv) and red bars represent the change of fluorescence signal after the introduction of $Hg^{2+}$ (1.0 equiv) to the above solution. (b) Fluorescence changes of 10 μM **PyRbO** in the presence of various metal ions in EtOH at 583 nm. Bars represent the final fluorescence intensity ($F_f$) over the initial fluorescence intensity ($F_i$) at $\lambda_{ex} = 515$ nm. Black bars represent the fluorescence intensity of 10 μM **PyRbO** with various competing metal ions (2.0 equiv) and red bars represent the change of fluorescence signal after the introduction of $Hg^{2+}$ (1.0 equiv) to the above solution. (For interpretation of the references to color in this figure legend, the reader is referred to the web version of this article.)

Ar–H), 8.02–7.97 (m, 2H, Ar–H), 7.48–7.40 (m, 2H, Ar–H), 7.07–7.00 (m, 2H, Ar–H), 6.79 (t, $J = 7.5$ Hz, 1H, Ar–H), 6.52 (d, $J = 8.9$ Hz, 3H, Ar–H), 6.39 (d, $J = 2.5$ Hz, 2H, Ar–H), 6.15 (dd, $J = 8.9$, 2.5 Hz, 2H, Ar–H), 5.95 (s, 2H, $CH_2$), 3.77 (t, $J = 5.7$ Hz, 2H, $CH_2$), 3.10 (q, $J = 7.1$ Hz, 8H, $CH_2$), 2.66 (t, $J = 7.4$ Hz, 2H, $CH_2$), 2.13–2.03 (m, 2H, $CH_2$), 0.97 (t, $J = 7.0$ Hz, 12H, $CH_3$). $^{13}C$ NMR (75 MHz, $CDCl_3$) δ 173.37, 157.08, 152.47, 148.81, 140.59, 128.22, 127.91, 127.79, 127.71, 127.21, 125.44, 124.52, 123.43, 122.83, 111.25, 108.01, 105.26, 97.85, 66.69, 64.79, 43.96, 30.80, 24.51, 12.38. TOF-MS: m/z 861.4 $[M + H]^+$, 883.6 $[M + Na]^+$.

### 2.2.6. Synthesis of thiooxorhodamine B hydrazide **4**

Lawesson's reagent (0.30 g, 0.75 mmol) was added in 5.0 mL toluene, and then the suspension was stirred under the atmosphere at 30 °C for 30 min. Compound **6** (0.57 g, 1.25 mmol) dissolved in 20 mL toluene was added to the reaction, and the reaction was refluxed at 85 °C. After 12 h, organic solvent was removed. 20 mL saturated solution of potassium carbonate was added to the residue, stirring for 2 h at room temperature, and then extracted by $CH_2Cl_2$. The organic phase was collected and removed. The crude product was purified by neutral alumina column chromatography (ethyl acetate/petroleum, 3:2, v/v) to afford compound **4** (0.23 g, yield: 39%). $^1H$ NMR (400 MHz, $CDCl_3$) δ 8.09 (d, $J = 4.7$ Hz, 1H, Ar–H), 7.47 (m, 2H, Ar–H), 7.12 (d, $J = 6.5$ Hz, 1H, Ar–H), 6.43 (d, $J = 2.5$ Hz, 2H, Ar–H), 6.35 (d, $J = 8.8$ Hz, 2H, Ar–H), 6.27 (dd, $J = 8.9$, 2.6 Hz, 2H, Ar–H), 4.82 (s, 2H, $NH_2$), 3.34 (q, $J = 7.1$ Hz, 8H, $CH_2$), 1.16 (t, $J = 7.1$ Hz, 12H, $CH_3$). TOF-MS: m/z 473.2 $[M + H]^+$.

### 2.2.7. Synthesis of probe compound **3**

Thiooxorhodamine B hydrazide **4** (0.41 g, 0.87 mmol) in 40 mL dry methyl alcohol was added. Salicylic aldehyde (0.13 g, 1.04 mmol) was added and then the reaction was refluxed at 50 °C. After 12 h, the appeared pink precipitate was filtered and washed 3 times with cold methyl alcohol. After drying, the reaction afforded 0.30 g solid in 74% yield. $^1H$ NMR (400 MHz, $CDCl_3$) δ 11.25 (s, 1H, OH), 8.70 (s, 1H, N═CH), 8.20–8.04 (m, 1H, Ar–H), 7.47–7.42 (m, 2H, Ar–H), 7.34–7.27 (m, 2H, Ar–H), 7.18–7.12 (m, 1H, Ar–H), 6.95 (d, $J = 8.2$ Hz, 1H, Ar–H), 6.90 (t, $J = 7.4$ Hz, 1H, Ar–H), 6.75 (d, $J = 8.8$ Hz, 2H, Ar–H), 6.40–6.23 (m, 4H, Ar–H), 3.32 (q, $J = 7.0$ Hz, 8H, $CH_2$), 1.15 (t, $J = 7.0$ Hz, 12H, $CH_3$). TOF-MS: m/z 577.3 $[M + H]^+$, 599.2 $[M + Na]^+$.

### 2.2.8. Synthesis of probe **2** (***PyRbS***)

Compound **3** (0.12 g, 0.2 mmol), compound **7** (0.23 g, 0.6 mmol), potassium carbonate (0.27 g, 2 mmol) and small amount of potassium iodide were mixed in 60 mL dry acetone and the mixture was stirred under reflux conditions for 12 h. The suspension was filtered, and then the solution was evaporated. The residue was purified by flash chromatography (EA/PE, 1:3, v/v) as eluant to afford 0.06 g light yellow product in a yield of 34%. $^1H$ NMR (400 MHz, $CDCl_3$) δ 8.97 (s, 1H, N═CH), 8.30 (d, $J = 9.2$ Hz, 1H, Ar–H), 8.19 (dd, $J = 7.5$, 3.0 Hz, 2H, Ar–H), 8.14 (dd, $J = 8.6$, 6.5 Hz, 3H, Ar–H), 8.07 (dd, $J = 8.5$, 6.6 Hz, 3H, Ar–H), 8.01 (dt, $J = 12.9$, 3.9 Hz, 2H, Ar–H), 7.43–7.32 (m, 2H, Ar–H), 7.20–7.14 (m, 1H, Ar–H), 7.11 (dd, $J = 7.5$, 0.8 Hz, 1H, Ar–H), 6.83 (t, $J = 7.6$ Hz, 1H, Ar–H), 6.76 (d,

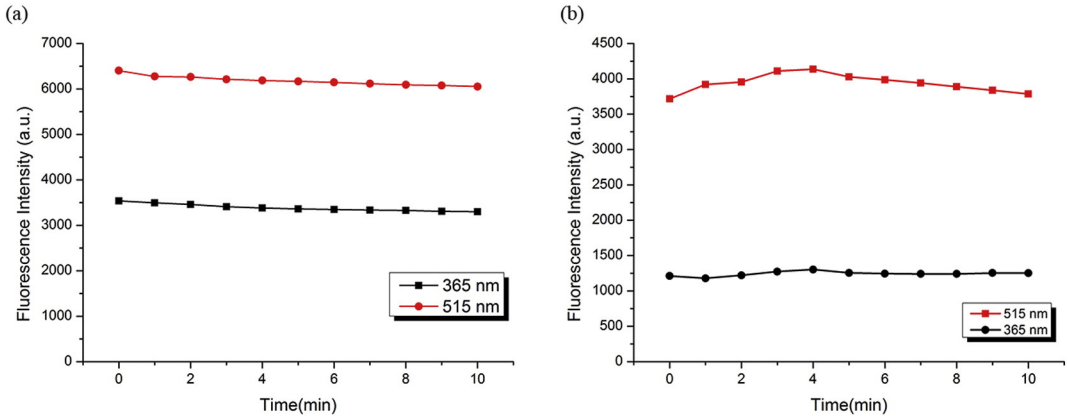


**Fig. 3.** (a) Fluorescence intensity of the response time of 5 μM **PyRbS** with $Hg^{2+}$ (1.0 equiv) in EtOH/$H_2O$ (2:1, v/v) at $\lambda_{em} = 592$ nm. (b) Fluorescence intensity of the response time of 10 μM **PyRbO** with $Hg^{2+}$ (1.0 equiv) in EtOH at $\lambda_{em} = 583$ nm.

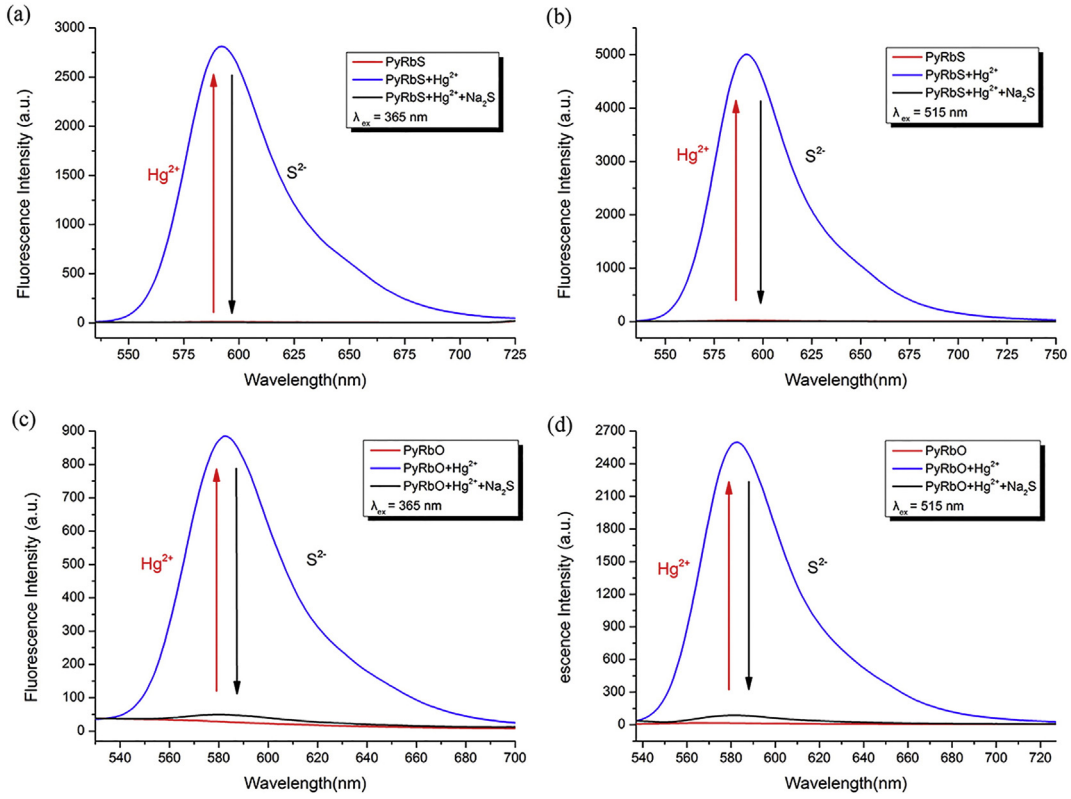


**Fig. 4.** (a) and (b) Reversibility of $Hg^{2+}$ to **PyRbS** (5 μM) by $Na_2S$ in EtOH/$H_2O$ (2:1, v/v). Red line: free **PyRbS** (5 μM), blue line: **PyRbS** + $Hg^{2+}$ (2.0 equiv), black line: **PyRbS** + $Hg^{2+}$ (2.0 equiv) + $S^{2-}$(4.0 equiv). (a) $\lambda_{ex} = 365$ nm. (b) $\lambda_{ex} = 515$ nm. (c) and (d) Reversibility of $Hg^{2+}$ to **PyRbO** (10 μM) by $Na_2S$ in EtOH. Red line: free **PyRbO** (10 μM), blue line: **PyRbO** + $Hg^{2+}$ (2.0 equiv), black line: **PyRbO** + $Hg^{2+}$ (2.0 equiv) + $S^{2-}$ (4.0 equiv). (c) $\lambda_{ex} = 365$ nm. (d) $\lambda_{ex} = 515$ nm.

*J* = 8.9 Hz, 2H, Ar–H), 6.70 (d, J = 8.3 Hz, 1H, Ar–H), 6.31 (d, *J* = 2.6 Hz, 2H, Ar–H), 6.25 (dd, *J* = 8.9, 2.6 Hz, 2H, Ar–H), 5.90 (s, 2H, $CH_2$), 4.01 (t, *J* = 6.0 Hz, 2H, $CH_2$), 3.30 (q, *J* = 7.0 Hz, 8H, $CH_2$), 2.66 (t, *J* = 7.1 Hz, 2H, $CH_2$), 2.20 (p, *J* = 6.6 Hz, 2H, $CH_2$), 1.13 (t, *J* = 7.0 Hz, 12H, $CH_3$). $^{13}C$ NMR (75 MHz, $CDCl_3$) δ 173.05, 171.23, 157.83, 155.17, 154.3, 151.71, 148.09, 131.96, 130.20, 128.19, 125.40, 124.55, 111.57, 110.55, 108.16, 97.37, 66.97, 64.76, 62.77, 44.26, 30.94, 24.57, 12.53. TOF-MS: m/z 877.5 $[M + H]^+$, 899.5 $[M + Na]^+$.

### 2.3. Fluorescence and UV–vis spectra experiments

Stock solutions of 10 mM **PyRbS** and **PyRbO** were prepared by dissolving in dimethyl sulphoxide. Stock solutions of 10 mM metal ions were prepared by dissolving in water. In our detecting experiments, the *fluorescence and UV–vis* response of **PyRbO** would be prevented with a certain amount of water in the experimental system. It was ascribed to the strong hydrolysis between the water and $Hg^{2+}$, which prohibited the ring opening of rhodamine B. However, the introduction

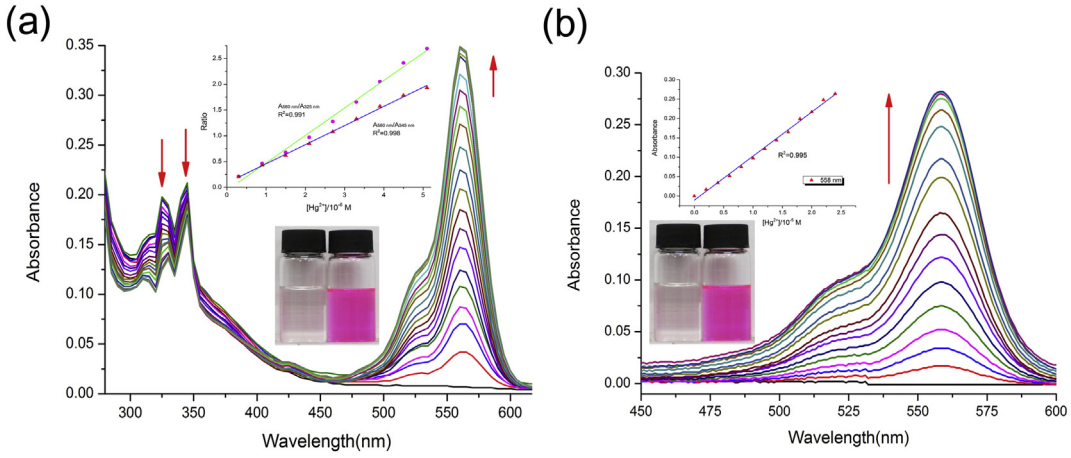


**Fig. 5.** (a) UV–vis absorption spectra of **PyRbS** (5 μM) in EtOH/$H_2O$ (2:1, v/v) with various amount of $Hg^{2+}$ (0–6 μM). Inset: The absorbance ratio of **PyRbS** at $A_{560\ nm}/A_{325\ nm}$ and $A_{560\ nm}/A_{345\ nm}$ as functions of the $Hg^{2+}$ concentration (0.3–5.1 μM) in EtOH/$H_2O$ (2:1, v/v) (top); the color change after the $Hg^{2+}$ introduction of **PyRbS** (bottom). (b) UV–vis titration of **PyRbO** (30 μM) in EtOH with various amount of $Hg^{2+}$ (0–35 μM). Inset: the absorbance at 558 nm of **PyRbO** (30 μM) as a function of the $Hg^{2+}$ concentration (2–24 μM) in EtOH (top); the color change after the $Hg^{2+}$ introduction of **PyRbO** (bottom).

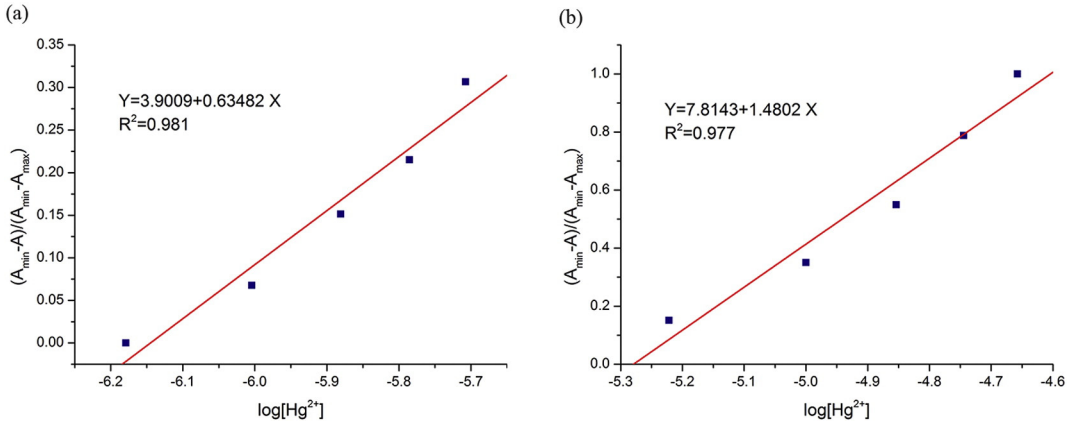


**Fig. 6.** (a) Absorbance of **PyRbS** in the different concentration of $Hg^{2+}$ in EtOH/$H_2O$ (2:1, v/v) at 560 nm, normalized between the minimum absorbance and the maximum absorbance intensity. The detection limit was calculated to be 0.72 μM. (b) Absorbance of **PyRbO** in the different concentration of $Hg^{2+}$ in EtOH at 558 nm, normalized between the minimum absorbance and the maximum absorbance intensity. The detection limit was calculated to be 5.3 μM.

of sulfur improved the complexation ability of **PyRbS** toward $Hg^{2+}$. Therefore, experiments of **PyRbS** were carried out in aqueous ethanol solution (EtOH/$H_2O$, 2:1, v/v), and experiments of **PyRbO** were in pure ethanol.

Appropriate amounts of different metal ions solution and **PyRbS** or **PyRbO** were added in 10 mL volumetric flasks by pipette, and then diluted with EtOH/$H_2O$ (v/v, 2:1) or ethanol to the calibration tail. The totally mixed resulting solutions were detected in a quartz optical cell with a 1 cm optical path length. For the fluorescence measurements, the excitation wavelength was set at 365 nm and 515 nm.

### 2.4. Confocal fluorescence imaging

MCF-7 cells (human breast carcinoma cells) were cultured in Dulbecco's modified Eagle medium (DMEM, Gibco) supplemented with 10% fetal bovine serum (FBS, Sigma), and penicillin (100 μg/mL) and streptomycin (100 μg/mL, Invitrogen) at 37 °C under 5% $CO_2$. One day before imaging, the cells were passed and plated on 24-well plates to 70% confluence. Subsequently, **PyRbS** (5 μM) in the culture media containing ethanol/PBS (1:49, v/v) was added to MCF-7 cells, which were incubated for 30 min. After the removal of extracellular extra **PyRbS** by washing for three times with PBS (phosphate buffered saline, pH = 7.2, Gibco), the cells were incubated with 5 μM $Hg^{2+}$ for 30 min at 37 °C and imaged by fluorescence microscopy (BX51, olympus, Japan).

### 2.5. Cytotoxicity experiments

The MTT (3-[4, 5-dimethylthiazol-2-yl]-2, 5-diphenyl tetrazolium bromide) assay was performed using A549 cells (human lung adenocarcinoma cells) to ascertain the cytotoxicity of **PyRbS**. A549 cells were seeded in 96-well cell-culture plate at 37 °C under 5% $CO_2$ before treatment. The cytotoxicity experiment was determined by MTT assay (Cell Proliferation Kit; keygen biological products, Nanjing, China), following the instructions of the kit. Briefly, A549 cells were treated with various concentrations (1, 5, 25, 50, 100 μM) of **PyRbS** and incubated 37 °C under 5% $CO_2$ for 24 h. Subsequently, MTT (5 mg/mL) was added to each well and incubated for 4 h. A microplate reader (SPECTRA SLT; Labinstruments, Salzburg, Austria) was used to measure the absorbance. The excitation wavelength was at 492 nm, and the emission was read at 690 nm. Each treatment was done in six wells, and the experiments were replicated three times. The control experiments were conducted under the identical conditions treated with DMEM plus 10% FBS and no-**PyRbS** added.

## 3. Results and discussion

### 3.1. The fluorescence spectra of probes

As shown in Fig. 1, the fluorescence properties of **PyRbS** (5 μM) and **PyRbO** (10 μM) were studied. **PyRbS** showed weak fluorescence without $Hg^{2+}$ in aqueous ethanol solution (EtOH/$H_2O$ = 2:1, v/v) due to

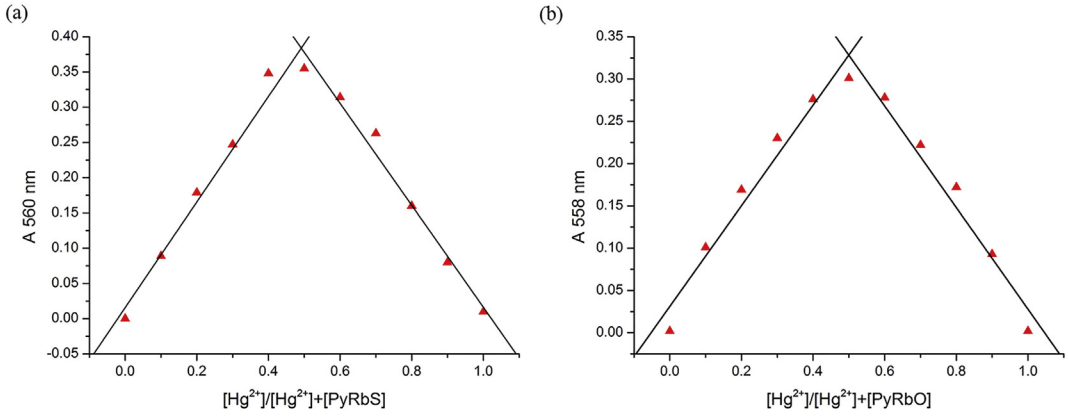


**Fig. 7.** (a) The Job's Plot of **PyRbS** with a total concentration of 10 μM ([**PyRbS**]+[$Hg^{2+}$]) in EtOH/$H_2O$ (2:1, v/v) at 560 nm. (b) The Job's Plot of **PyRbO** with a total concentration of 60 μM ([**PyRbO**]+[$Hg^{2+}$]) in EtOH at 558 nm.

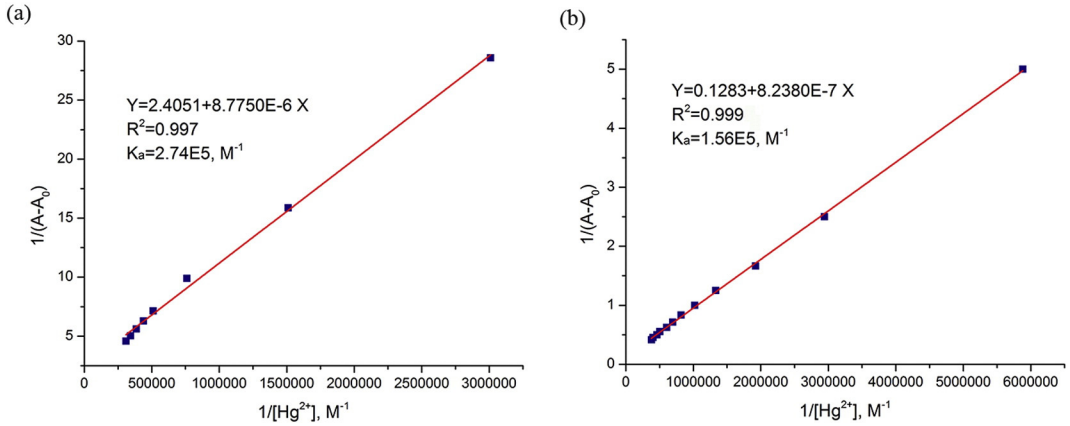


**Fig. 8.** (a) Benesi–Hilderbrand plot of **PyRbS** with $Hg^{2+}$. (b) Benesi–Hilderbrand plot of **PyRbO** with $Hg^{2+}$.

the spirothiocyclic formation. When the $Hg^{2+}$ was introduced, significant bands at 592 nm ($\lambda_{ex}$ = 365 nm and 515 nm) (Fig. 1a and b) were gradually appeared. The emission color was changed from colorless to bright orange, which could be observed by naked eye. This was also attributed to the ring opening process of the rhodamine derivatives [23]. The fluorescence signal at 592 nm increased with $Hg^{2+}$ concentration, and reached a maximum with 5 μM of $Hg^{2+}$. A nearly linear relationship ($R^2$ = 0.999) was observed with $Hg^{2+}$ concentrations from 0.3 to 4.8 μM ($\lambda_{ex}$ = 365 nm). Similarly, linear fluorescent response ($R^2$ = 0.997) to $Hg^{2+}$ ranging from 0.3 to 5.4 μM was also obtained when emission wavelength was 515 nm. In the case of **PyRbO**, remarkable enhancement of fluorescence intensity at 583 nm ($\lambda_{ex}$ = 365 nm and 515 nm) (Fig. 1c and d) and the obvious change of color which is from colorless to reddish-orange were observed. The linear relationships between fluorescence intensity and $Hg^{2+}$ concentrations ($\lambda_{ex}$ = 365 nm, 2–16 μM $Hg^{2+}$, $R^2$ = 0.984; $\lambda_{ex}$ = 515 nm, 6–16 μM $Hg^{2+}$, $R^2$ = 0.990) were also obtained. Taken together, **PyRbS** had better linear relationship with low concentration $Hg^{2+}$, compared with **PyRbO**.

Moreover, the fluorescence spectra of **PyRbS** (5 μM) and **PyRbO** (10 μM) in the presence of various metal ions ($Na^+$, $K^+$, $Ca^{2+}$, $Mg^{2+}$, $Ni^{2+}$, $Ba^{2+}$, $Ag^+$, $Zn^{2+}$, $Mn^{2+}$, $Cu^{2+}$, $Cd^{2+}$, $Pb^{2+}$, $Cr^{3+}$, $Co^{2+}$, $Al^{3+}$ and $Fe^{2+}$) were separately studied (Fig. 2). Free **PyRbS** showed almost no fluorescence at 592 nm ($\lambda_{ex}$ = 515 nm) in ethanol aqueous solution (EtOH/$H_2O$ = 2:1, v/v). Then these metal ions (4.0 equiv) were introduced. In the solution of **PyRbS**, alkali metal ions ($K^+$, $Na^+$), alkali-earth metal ions ($Mg^{2+}$, $Ca^{2+}$) had negligible influence and $Ag^+$, $Fe^{2+}$, $Cr^{3+}$ and $Al^{3+}$ caused slight fluorescence variation. Similarly, free **PyRbO** also showed very low fluorescence in pure ethanol and a few metal ions ($Ag^+$, $Zn^{2+}$, $Cu^{2+}$ $Cr^{3+}$, $Al^{3+}$, $Fe^{2+}$) (2.0 equiv) could result in small fluorescence intensity changes. To further evaluate the selectivity of the probes for $Hg^{2+}$, metal ions competition experiments (including $Hg^{2+}$ and other ions) were also investigated under identical conditions. The addition of only $Hg^{2+}$ (1.0 equiv) caused obvious fluorescence change in the solution of **PyRbS** or **PyRbO** and metal ions. As shown in bar graphs, there was no obvious fluorescence intensity variation of probes/$Hg^{2+}$ complex comparing the results with/without other metal ions. These results clearly demonstrated that these metal ions could not interfere with the detection of $Hg^{2+}$. Thus, **PyRbS** and **PyRbO** could be used as selective $Hg^{2+}$ probes.

Response time experiments of **PyRbS**/$Hg^{2+}$ and **PyRbO**/$Hg^{2+}$ system were also studied. $Hg^{2+}$ (1.0 equiv) was separately added to two optical quartz cells with 1 cm path length containing 5 μM **PyRbS** in EtOH/$H_2O$ (2:1, v/v) and 10 μM **PyRbO** in EtOH. Excitation wavelength was 515 nm and emission wavelengths were 592 nm (**PyRbS**) and 583 nm (**PyRbO**), respectively. The changes of fluorescence intensity were recorded. As shown in Fig. 3, both **PyRbS** and **PyRbO** completed the complexation progress with $Hg^{2+}$ within a short time. Fluorescence signal could be detected immediately after the introduction of $Hg^{2+}$ to probe solution. Therefore, **PyRbS** and **PyRbO** did not need long time for equilibrium before detecting, and they could be used in real time detection of $Hg^{2+}$.

The reversibility is an important property of chemosensor, and mercury is sulphophile element (the $K_d$ value of $[HgS^{2-}]^{2-}$ is $10^{-50}$ $M^2$) [24]. Then $Na_2S$-addition experiments were conducted to examine the reversibility of **PyRbS** and **PyRbO** with $Hg^{2+}$ (Fig. 4). The results displayed that the fluorescence enhancement caused by $Hg^{2+}$-addition (2.0 equiv) declined to the initial fluorescence intensity after the addition of $Na_2S$ solution (4.0 equiv) ($\lambda_{ex}$ = 365 nm and 515 nm), and the color of them faded to the pink color. The fluorescence spectra

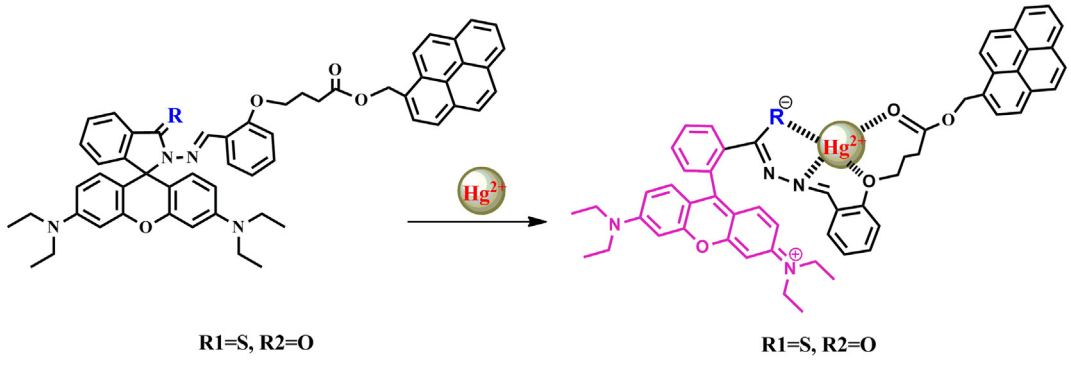


**Scheme 2.** Proposed binding mechanism of **PyRbO** and **PyRbO** with $Hg^{2+}$.

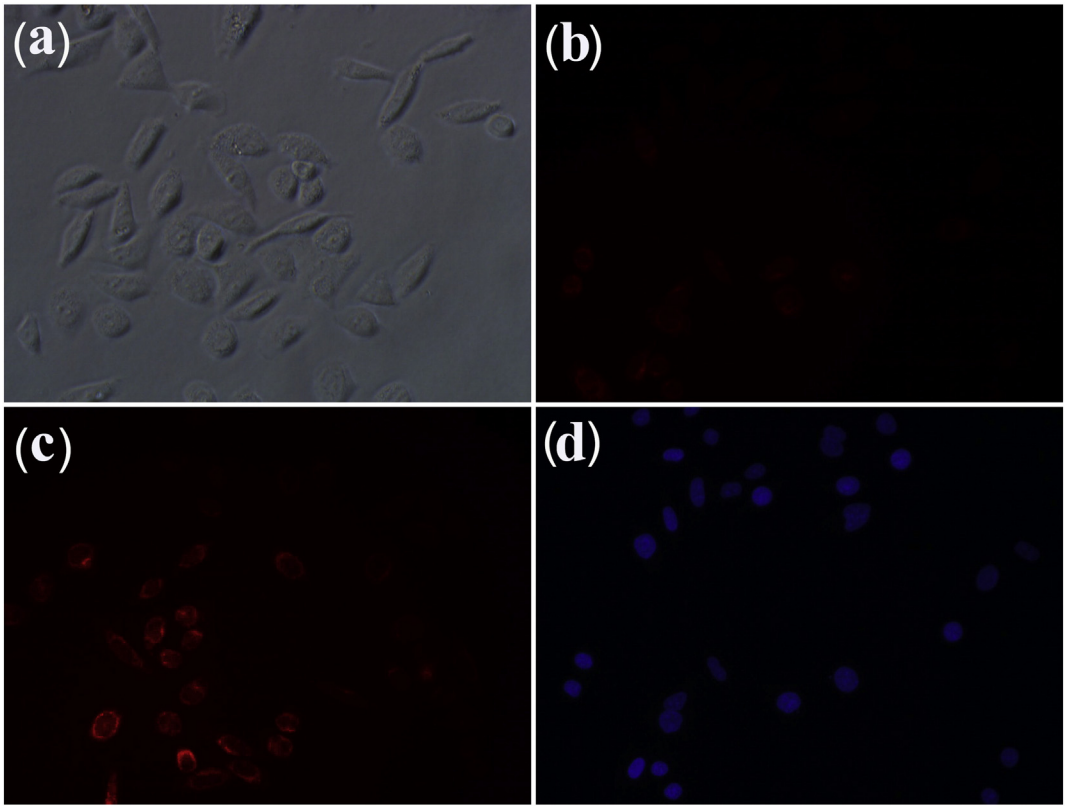


**Fig. 9.** Confocal fluorescence images in MCF-7 cells. (a) Brighe-field image. (b) Cells stained with **PyRbS** (5 μM) for 30 min. (c) subsequently exposed to $Hg^{2+}$ for 30 min. (d) cell nucleus labeled with Hoechst 33342.

were observed, indicating that **PyRbS** had a better reversibility. Therefore, both **PyRbS** and **PyRbO** were reversible of detecting $Hg^{2+}$.

### 3.2. The UV–vis spectra of probes

The changes of the UV–vis spectroscopy titration for **PyRbS** (5 μM) with the increasing amounts of $Hg^{2+}$ in aqueous solution (EtOH/$H_2O$ = 2:1, v/v) were recorded in Fig. 5a. Besides, analog compound **PyRbO** (30 μM) was detected in absolute ethanol in the same way (Fig. 5b). The absorption of both **PyRbS** and **PyRbO** in the absence of $Hg^{2+}$ was weak from 450 to 600 nm, which indicated that the spirolactam rhodamine form was the dominant species. Upon the addition of $Hg^{2+}$, there were obvious absorption peaks at 560 nm (**PyRbS**) and 558 nm (**PyRbO**) respectively (**PyRbS**, $\varepsilon = 6.71 \times 10^4$ L $mol^{-1}$ $cm^{-1}$; **PyRbO**, $\varepsilon = 1.06 \times 10^4$ L $mol^{-1}$ $cm^{-1}$) and their color changed from colorless to pink, suggesting the formation of ring-opened rhodamine species. Additionally, ratiometric changes in the absorption spectra of **PyRbS** were observed. Free **PyRbS** showed pyrene absorptions at 324 nm and 345 nm, which decreased gradually after the addition of $Hg^{2+}$. A near linear dependence of the ratio of $A_{560\ nm}/A_{325\ nm}$ (blue line, $R^2 = 0.991$) and the ratio of $A_{560\ nm}/A_{345\ nm}$ (green line, $R^2 = 0.998$) as functions of $Hg^{2+}$ ion concentration (0.3–5.1 μM) were obtained. The ratios changed from 0.21 to 2.69 and 0.20 to 1.93 respectively. This indicated the capability of **PyRbS** for quantitatively detecting $Hg^{2+}$ by being a ratiometric probe, which has the important feature in that it permits signal rationing and thus increases the dynamic range and provides built-in correction for environmental effects [25]. A nearly linear relationship ($R^2 = 0.995$) of **PyRbO** was observed with $Hg^{2+}$ concentrations from 2 to 24 μM.

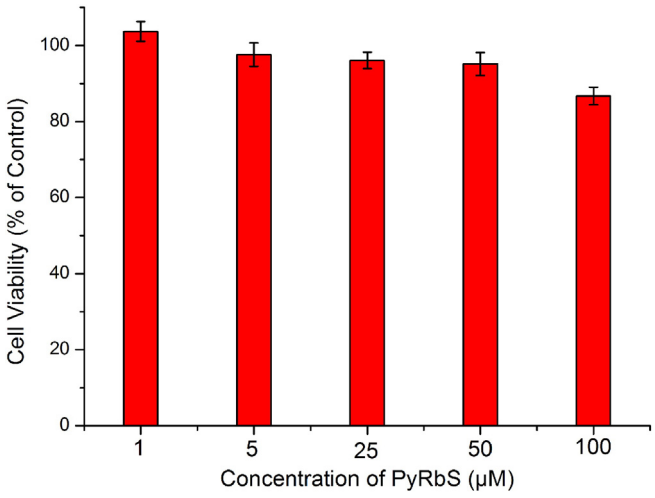


**Fig. 10.** Cell viability (%) of A549 cells cultured in the presence of **PyRbS** (0–100 μM) at 37 °C for 24 h.

Besides, the UV–vis titration data were used to calculated the detection limit according to a reported method [26,27]. Absorbance of **PyRbS** and **PyRbO** in the different concentration of $Hg^{2+}$ at the maximum absorption wavelength was normalized between the minimum absorbance and the maximum absorbance intensity. Then the normalized absorbance was linearly proportional to log[$Hg^{2+}$] ($y = A + Bx$) (Fig. 6). The detection limit value was obtained from $10^{-A/B}$. The detection limit of **PyRbS** was calculated to be 0.72 μM (Fig. 6a), while that of **PyRbO** was 5.3 μM (Fig. 6b). These observations clearly indicated that both **PyRbS** and **PyRbO** could be used for quantitative detection of $Hg^{2+}$. Obviously, **PyRbS** had advantages over **PyRbO** not only because of its higher molar absorption coefficient and lower detection limit, but also the capability of **PyRbS** for ratio measurements, which could eliminate the errors caused by the concentration of probe molecules, surrounding environment and other factors.

Job's Plot analysis was used to figure out the stoichiometry for **PyRbS**/$Hg^{2+}$ and **PyRbO**/$Hg^{2+}$ complex. The Job's Plot was conducted by using absorption of the probes and $Hg^{2+}$ at the maximum absorption wavelength plotted against continuous variation with a total concentration of 10 μM ([**PyRbS**]+[$Hg^{2+}$]) and 60 μM ([**PyRbO**]+[$Hg^{2+}$]) (Fig. 7). The results of the both Job's Plots exhibited the same maximum absorbance when the molar fraction of [$Hg^{2+}$]/([$Hg^{2+}$]+[probe]) was 0.5, indicating a 1:1 stoichiometry. On the basis of the 1:1 stoichiometry and UV–vis titration date, the association constants ($K_a$) of the two probes with $Hg^{2+}$ were calculated using the Benesi–Hildebrand method [28], which was derived as the following formula [29]:

$$1/(A-A_0) = [a/(a-b)]\left[1 + 1/\left(K_a\left[Hg^{2+}\right]\right)\right]$$

where A is the obtained absorbance of probes at the maximum absorption wavelength after the addition of $Hg^{2+}$, and $A_0$ stands for the initial absorbance of free probes. A linear relationship was obtained ($R^2_{\mathbf{PyRbS}} = 0.997$, $R^2_{\mathbf{PyRbO}} = 0.999$), when the $1/(A-A_0)$ was plotted as a function of $1/[Hg^{2+}]$ ($y = A + Bx$) (Fig. 8), which further proved the 1:1 stoichiometry. The association constant value was calculated as $2.74 \times 10^5\ M^{-1}$ (**PyRbS**/$Hg^{2+}$) and $1.56 \times 10^5\ M^{-1}$ (**PyRbO**$Hg^{2+}$) respectively from A/B.

From the foregoing conclusions, the spectral response of **PyRbS** or **PyRbO** to $Hg^{2+}$ elicited by the reversible binding events were likely due to the chelation-induced ring-opening of the rhodamine spirolactam. The possible structures of this reversible process were shown in Scheme 2.

Taking all the aforementioned in consideration, it was found that **PyRbS** was superior to **PyRbO** owing to its higher molar absorption coefficient, higher association constant and lower detection limit in aqueous solution. Moreover, **PyRbS** could be used for detecting $Hg^{2+}$ quantitatively by ratiometric absorption measurement. These superior properties of **PyRbS** were presumably ascribed to the thiophilic nature of $Hg^{2+}$, which had been confirmed from reported references [30]. Owing to its favorable molecular properties, **PyRbS** should be suited for $Hg^{2+}$ monitoring in living cells. Therefore, imaging and cytotoxicity experiments were performed.

### 3.3. Live-cell imaging

To investigate the property of the probe **PyRbS** for detecting $Hg^{2+}$ in living cells, fluorescence images of MCF-7 cells observed under the confocal microscope (Fig. 9). MCF-7 cells were incubated with **PyRbS** (5 μM) for 30 min at 37 °C showed very weak intracellular fluorescence (Fig. 9b). However, a much brighter red fluorescence from the intracellular area was observed after the introduction of $Hg^{2+}$ (5 μM) in (Fig. 9c). Bright-field image after $Hg^{2+}$ and **PyRbS** treatment confirmed the viability of the cells over the course of the imaging experiments (Fig. 9a). Furthermore, the image of fluorescence microscopy of cells stained with **PyRbS**/$Hg^{2+}$ and Hoechst 33342 was shown in Fig. 9d. The result indicated that **PyRbS** was cell-membrane permeable, and $Hg^{2+}$ predominantly existed in the perinuclear area.

### 3.4. Cytotoxicity experiments

Thiazolyl Blue Tetrazolium Bromide (MTT) assay was applied to measure the cytotoxicity of **PyRbS** in human pulmonary adenocarcinoma cell (A549 cells). The cell viability (%) was calculated according to the following equation:

$$\text{cell viability (\%)} = OD_{sample} / OD_{control} \times 100$$

where $OD_{sample}$ is the mean of optical densities of the wells treated with different concentrations of probe **PyRbS**, and $OD_{control}$ represents the mean of optical densities of the control group. The reported percent cell survival values are relative to untreated control cells. As shown in Fig. 10, the cell viability was estimated to be more than 85% upon **PyRbS** treatment after 24 h, which indicated the low cytotoxicity even at concentration of **PyRbS** as high as 100 μM. Both cell imaging and cell viability examination suggested that **PyRbS** was biocompatible with living cells. It was noticeable that the concentration of **PyRbS** (5 μM) used for cell imaging was much lower than that for cell viability testing (100 μM), suggesting its potential for biological imaging application.

## 4. Conclusion

In summary, we have successfully prepared two colorimetric and fluorometric probes **PyRbS** and **PyRbO** based on rhodamine B and pyrene for the detection of $Hg^{2+}$. These two probes showed high selectivity to $Hg^{2+}$. The stoichiometric ratio of probes and $Hg^{2+}$ was 1:1, and changes of color were obvious under visible under visible and UV light, which could be used for naked-eye detection. Compared with **PyRbO**, **PyRbS** exhibited better spectral properties, including higher selectivity, advantageous reversibility, and lower detection limit, due to the thiophilic property of $Hg^{2+}$ ion. Furthermore, pyrene moiety served successfully as a source of ratiometric absorption changes of **PyRbS** with $Hg^{2+}$, which showed the capability of **PyRbS** for calibrating and determining $Hg^{2+}$ by absorption ratio measurement. Additionally, confocal fluorescence images and cytotoxicity experiment indicated that **PyRbS** could be potential candidate for detecting $Hg^{2+}$ in biological system.

## Acknowledgments

This work is supported by the Open Fund of the State Key Laboratory of Materials-Oriented Chemical Engineering (KL13-07), the Open Fund of the State Key Laboratory of Coordination Chemistry, the Postgraduate Education and Innovation Project of Jiangsu Province (KYLX-0772), the Specialized Research Fund for the Doctoral Program of Higher Education (20123221110012), and the China Postdoctoral Science Foundation (2014M550287).

## Appendix A. Supplementary data

Supplementary data to this article can be found online at http://dx.doi.org/10.1016/j.saa.2016.01.024.

## References

[1] E.M. Nolan, S.J. Lippard, Chem. Rev. 108 (2008) 3443–3480.
[2] A. Renzoni, F. Zino, E. Franchi, Environ. Res. 77 (1998) 68–72.
[3] D. Zhang, J. Su, X. Ma, H. Tian, Tetrahedron 64 (2008) 8515–8521.
[4] D.L. Godbold, A. Hüttermann, Physiol. Plant. 74 (1988) 270–275.
[5] I. Terashima, K. Ono, Plant Cell Physiol. 43 (2002) 70–78.
[6] E.G. Malcolm, J.K. Schaefer, E.B. Ekstrom, C.B. Tuit, A. Jayakumar, H. Park, B.B. Ward, F.M.M. Morel, Mar. Chem. 122 (2010) 11–19.
[7] J.K. Schaefer, F.M.M. Morel, Nat. Geosci. 2 (2009) 123–126.
[8] S.A. Counter, L.H. Buchanan, Toxicol. Appl. Pharmacol. 198 (2004) 209–230.
[9] P.M. Bolger, B.A. Schwetz, N. Engl. J. Med. 347 (2002) 1735–1736.
[10] J.F. Nyland, S.B. Wang, D.L. Shirley, E.O. Santos, A.M. Ventura, J.M. de Souza, E.K. Silbergeld, Environ. Res. 111 (2011) 584–589.
[11] M. Lombardo, I. Vassura, D. Fabbri, C. Trombini, J. Organomet. Chem. 690 (2005) 588–593.
[12] L. Liu, W.-Y. Wong, Y.-W. Lam, W.-Y. Tam, Inorg. Chim. Acta 360 (2007) 109–121.
[13] L. Liu, Y.-W. Lam, W.-Y. Wong, J. Organomet. Chem. 691 (2006) 1092–1100.
[14] I. Medina, E. Rubí, M.C. Mejuto, R. Cela, Talanta 40 (1993) 1631–1636.
[15] S. Saito, S. Sasamura, S. Hoshi, Analyst 130 (2005) 659–663.
[16] P. Kubáň, P. Houserová, P. Kubáň, P.C. Hauser, V. Kubáň, J. Sep. Sci. 30 (2007) 1070–1076.
[17] R. Cervenka, Zelinkov, Aacute, Hana, Konecn, Aacute, Marie, Kom, Aacute, J. Rek, Anal. Sci. 26 (2010) 989–993.
[18] E. Stanisz, J. Werner, H. Matusiewicz, Microchem. J. 110 (2013) 28–35.
[19] R. Martínez-Máñez, F. Sancenón, Chem. Rev. 103 (2003) 4419–4476.
[20] D.T. Quang, J.S. Kim, Chem. Rev. 110 (2010) 6280–6301.
[21] R. Álvarez, B. Vaz, H. Gronemeyer, Á.R. de Lera, Chem. Rev. 114 (2013) 1–125.
[22] Z. Zeng, A.A.J. Torriero, A.M. Bond, L. Spiccia, Chem. Eur. J. 16 (2010) 9154–9163.

[23] X. Chen, T. Pradhan, F. Wang, J.S. Kim, J. Yoon, Chem. Rev. 112 (2011) 1910–1956.
[24] R.D. Armstrong, D.F. Porter, H.R. Thirsk, J. Phys. Chem. 72 (1968) 2300–2306.
[25] Z. Xu, Y. Xiao, X. Qian, J. Cui, D. Cui, Org. Lett. 7 (2005) 889–892.
[26] W. Lin, L. Yuan, Z. Cao, Y. Feng, L. Long, Chemistry 15 (2009) 5096–5103.
[27] Y.S. Mi, Z. Cao, Y.T. Chen, Q.F. Xie, Y.Y. Xu, Y.F. Luo, J.J. Shi, J.N. Xiang, Analyst 138 (2013) 5274–5280.
[28] X.-B. Yang, B.-X. Yang, J.-F. Ge, Y.-J. Xu, Q.-F. Xu, J. Liang, J.-M. Lu, Org. Lett. 13 (2011) 2710–2713.
[29] M. Zhu, M. Yuan, X. Liu, J. Xu, J. Lv, C. Huang, H. Liu, Y. Li, S. Wang, D. Zhu, Org. Lett. 10 (2008) 1481–1484.
[30] K.-H. Chu, Y. Zhou, Y. Fang, L.-H. Wang, J.-Y. Li, C. Yao, Dyes Pigments 98 (2013) 339–346.